ACS APPLIED MATERIALS & INTERFACES

Research Article

www.acsami.org

Photochemical Synthesis of Noble Metal (Ag, Pd, Au, Pt) on Graphene/ZnO Multihybrid Nanoarchitectures as Electrocatalysis for H_2O_2 Reduction

Hui Gu, Yan Yang, Jixiang Tian, and Guoyue Shi*

Department of Chemistry, East China Normal University, 500 Dongchuan Road, Shanghai, 200241, P.R. China

Supporting Information

ABSTRACT: For the first time, a series of noble metal (Ag, Au, Pd, and Pt) nanoparticles (NPs) based on new functional graphene were successfully achieved via UV-assisted photocatalytic reduction by ZnO nanorods. The whole preparation strategy for constructing noble metal deposited graphene sheets/ZnO (GS/ZnO) was elucidated in detail in this work. First, graphene oxide based two-dimensional carbon nanostructures served as a support to disperse ZnO nanorods through a hydrothermal route. The ZnO nanorods were self-assembled onto the surface of graphene sheets, forming GS/ZnO nanocomposite, and the graphene oxide was reduced, yielding reduced graphene sheets in this synthetic procedure. Second, the GS/ZnO films were further employed as supporting materials for the dispersion of metal nanoparticles. Photogenerated electrons from UV-irradiated ZnO were transported across GS to stepwise and respectively reduce v μL metal ions (Ag^+, Pd^{2+}, $AuCl_4^-$, $PtCl_6^{2-}$, 20 mg/mL) into metal (Ag, Pd, Au, Pt) NPs at a location distinct from the ZnO anchored site, forming five graphene-based hybrid nanocomposites designated as GS/ZnO, GS/ZnO@Ag_v, GS/ZnO@Pd_v, GS/ZnO@Au_v, GS/ZnO@Pt_v, respectively. The obtained mutihybrid nanoarchitectured materials were clearly characterized by transmission electron microscopy (TEM) and X-ray diffraction (XRD). According to the diameters and distribution, the four metal NPs on GS/ZnO were divided into two categories: Ag&Au and Pd&Pt. Their difference was rooted in the rival abilities of gathering electron between graphene and different metal islands in the photochemical reduction process. The electrochemical behaviors of the five resultant hybrid nanocomposites were investigated in H_2O_2 as well as in potassium ferricyanide ($Fe(CN)_6^{3-/4-}$) and displayed distinct electrocatalytic activity.

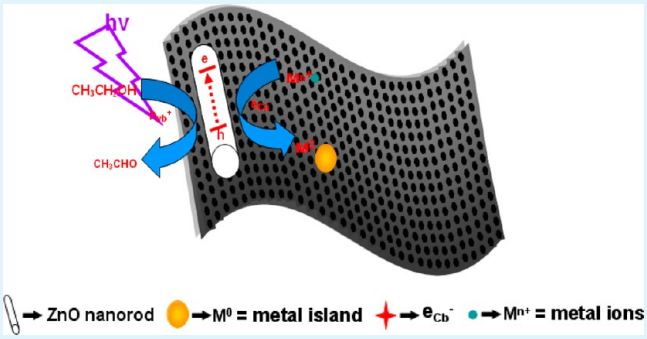

KEYWORDS: *graphene, ZnO, photocatalyst, metal nanoparticle, electron storage, electrocatalyst*

INTRODUCTION

Hybrid nanocomposite materials with synergies different components show distinguished performance in optics, electronics, catalysis, and other applications.[1,2] In recent years, metal−semiconductor hybrids with improved functionality were intensively investigated[3,4] with many developed ways, such as chemical and electrochemical metal deposition, electrostatical metal deposition, metal sputtering, and so forth. Among them, photochemical synthesis of metal−semiconductor hybrids has attracted considerable attention in recent years due to its advantages of comparatively mild synthesis conditions, favorable prerequisites for the formation of tight electronic contact between the components, and well controllable kinetics.[5,6] ZnO, because of its transparency in the visible range, environmental and electrical stability, direct energy band gap of 3.37 eV with a large excitation binding energy of 60 meV, and so forth, was intensively used as the semiconductor for metal deposition with photochemistry.[7,8] For example, a new route to site-specific growth of Au particles on ZnO nanopyramids under ultraviolet illumination has been developed by Han'group.[9] Claudia and co-workers synthesized the site-specific Ag nanoparticles on ZnO nanorods through anisotropic photoreduction of Ag^+ ions.[10]

Graphene has become a rising star because of its one atom thick and 2D layers of sp^2-hybridized carbon structure.[11,12] Unique properties, such as high specific surface areas of ∼2600 m^2/g,[13] high thermal conductivity, and excellent electronic mobility,[14,15] are opening a wide variety of applications in the fields of capacitors, sensors, devices, drug delivery, and solar cells.[16−20] Specially, the ability of RGO to store and shuttle electrons, as visualized via a stepwise electron transfer process, demonstrates its capability to serve as a catalyst nanomaterial and to transfer electrons on demand to adsorbed species. Using reduced graphene oxide (RGO) as a two-dimensional support, Kamat and co-workers prepared the TiO_2−graphene nanocomposites through the UV-assisted photocatalytic reduction of

Received: May 10, 2013
Accepted: June 22, 2013
Published: June 22, 2013

   dx.doi.org/10.1021/am401738k | ACS Appl. Mater. Interfaces 2013, 5, 6762−6768

Scheme 1. Schematic for the Procedures of the Preparations of (i) GS/ZnO and (ii) GS/ZnO@Pd/Pt and GS/ZnO@Ag/Au[a]

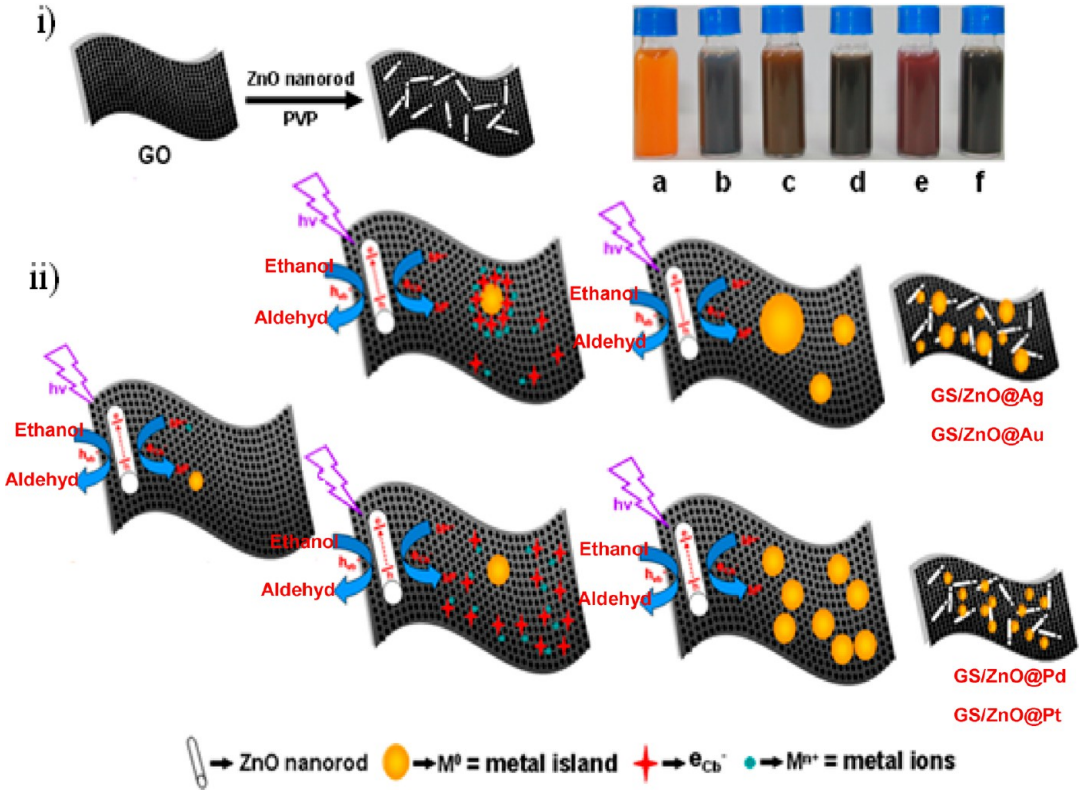

[a]Inset: digital photographs of (a) GO, (b) GS/ZnO, (c) GS/ZnO@Ag, (d) GS/ZnO@Pd, (e) GS/ZnO@Au, and (f) GS/ZnO@Pt.

graphene oxide, which is suspended in ethanol undergoing reduction as it accepts electrons from UV-irradiated TiO_2.[21] Continuously, they also succeeded in selective anchoring of semiconductor and metal nanoparticles at separate sites. Photogenerated electrons from UV-irradiated TiO_2 are transported across RGO to reduce silver ions into silver nanoparticles at a location distinct from the TiO_2 anchored site.[22] Large-area reduced graphene oxide−ZnO thin film suspensions were fabricated and patterned by Liua et al. with a mild photoassisted reduction method, and its photocatalytic performance in reduction of Cr(VI) was enhanced.[23] Therefore, through the photoelectric reduction, the electrons photoexcited from ZnO can be transferred into GS and combined with metal ions to produce metal nanoparticles (NPs), which provide a convenient route to successfully embed the resultant metal NPs with varied diameters on the GS/ZnO films.

Herein, positively charged ZnO nanorods were first self-assembled onto the surface of negatively charged graphene oxide forming GS/ZnO nanocomposite through a hydrothermal route in the presence of poly(*N*-vinyl-2-pyrrolidone) (PVP). Consequently, ZnO nanorods functionalized GS were achieved with improved water solubility and enhanced electrical conductivity. Then, the GS/ZnO was dispersed in polar solvents and exposed to UV light ($\lambda \approx 265$ nm). The photocatalytic reduction of metal ions (Ag^+, Pd^2+, $AuCl_4^-$, $PtCl_6^{2-}$) to metal (Ag, Pd, Au, Pt) NPs occurred, and the resultant metal NPs were embedded on the GS/ZnO films with varied diameters as a function of the feeding volume of the reductant. Finally, five graphene-based hybrid nanocomposites were prepared and designated as GS/ZnO, GS/ZnO@Ag_v, GS/ZnO@Pd_v, GS/ZnO@Au_v, and GS/ZnO@Pt_v. We interestingly found that the morphology as well as the distribution of the resultant for four GS/ZnO@M_v films obtained through a photoelectric reduction process fell into two categories: Ag&Au and Pd&Pt. Their difference was rooted in the rival abilities of gathering electron between graphene and different metal islands in the photochemical reduction process. Moreover, it was reported that incorporation of two or more catalyst particles onto an individual graphene or reduced graphene oxide sheet at separate sites can provide greater versatility in carrying out selective catalytic or sensing processes.[24] Therefore, further electrochemical research including electrochemical characteristics and electrochemical activities toward the reduction to H_2O_2 of the five as-prepared graphene-based hybrid nanocomposites has also been systematically discussed in this work.

RESULTS AND DISCUSSION

Characterization of GS/ZnO@M_{380} Nanocomposites. To reveal the metal NPs spreading on the GS clearly, GS/ZnO composite was synthesized as the mass ratio of 1:2 and then dissolved in ethanol (5 mg/mL). Upon UV irradiation, a solution-based stepwise electron transfer process was conducted as shown in Scheme 1. The first step involved one charge separation in ZnO nanorods using UV irradiation ($\lambda \approx 265$ nm), forming electron−hole pairs. In the presence of ethanol, the holes were scavenged to produce ethoxy radicals, thus leaving the electrons to accumulate within graphene. Second, the stored electrons were then transferred to the additive metal ions (Ag^+, Pd^{2+}, $AuCl_4^-$, $PtCl_6^{2-}$) and allowed the reduction of metal ions to form metal (Ag, Pd, Au, Pt) islands on the surface of graphene. Third, as irradiation continued, the excitated electrons competed for storing within GS or gathering

around the deposited metal islands. The electrons in GS were scavenged by metal ions to produce new metal islands, while the electrons gathered around the previous metal islands were captured by additive metal ions, thus making these metal islands grow. In the presence of coinage coinage metals islands, such as Ag and Au, electrons accumulate and pass to the islands where they are stored,[25,26] which endows the growth of the primary metal islands. However, unlike the coinage metals, most potent hydrogenation catalysts, such as Pd and Pt, do not display strong plasmon bands in the UV−vis region, which is due to the damping effect of the d−d transitions in these metals and thus tends to wash out the free electron contribution to the dielectric function.[27] Therefore, the electrons are stored in graphene to facilitate the deposition of growing new metal islands at different sites on the GS/ZnO surface.

Figure 1 displays the representative TEM images for GS/ZnO@ M_{380} hybrid nanocomposites at low (Figure 1a−d) and high magnifications (Figure 1e−h). It is evident that metal NPs are deposited on GS with high-contrast to ZnO nanorods, and their sizes and distributions vary from each other. As revealed in HRTEM images (Figure 1e−h), the lattice spacing of the Ag, Pd, Au, and Pt nanocrystals are about 0.24, 0.23, 0.24, and 0.23 nm, respectively, corresponding to single crystals of Ag, Pd, Au, and Pt all with many (111) facets,[28−31] It confirms that the black dots seen from the TEM images are the relevant metal NPs other than ZnO nanorods.

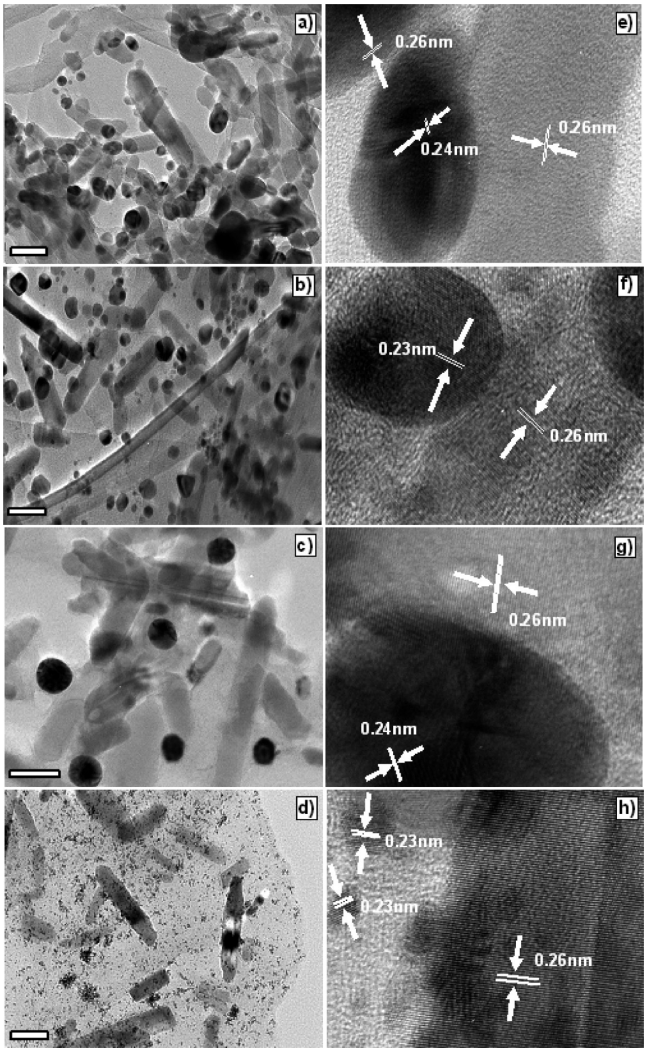

Figure 1. Typical TEM images of (a) GS/ZnO@Ag_{380}, (b) GS/ZnO@Pd_{380}, (c) GS/ZnO @Au_{380}, and (d) GS/ZnO@Pt_{380}; HRTEM images of the interface of (e) Ag NPs, (f) Pd NPs, (g) Au NPs, and (h) Pt NPs and ZnO nanorods. All scale bars shown represent 50 nm.

From Figure 1, we also can see that the diameters of Ag NPs range from 12 to 34 nm while the sizes of Au NPs are varied from 20 to 36 nm, which is due to easy accumulation electrons of the Ag and Au islands thus in favor of the Ag and Au islands growth. More importantly, the Au islands are easier to pile up electrons than Ag, thus making the size of Au NPs are larger than that of Ag. The mechanism is further demonstrated by continuous addition of 200 μL Ag^+ and $AuCl_4^-$ solution into the reaction system. As shown in Figure 2a and c, a part of the small Ag and Au NPs are still exist, however, most of them reach the sizes larger about 50 nm and 80 nm respectively. Compared with that of Ag and Au NPs, the growth and topography of Pd and Pt NPs are definitely different. In Figure 1b and d, we can see that the Pd and Pt NPs are relatively uniformly distributed on GS/ZnO films with no agglomeration and are well isolated from each other. The diameter of Pd NPs is from 5 to 23 nm and that of the Pt NPs is 2−3 nm, which are much smaller than Ag and Au. The reason is the two islands of Pd and Pt have the tendency to wash out the free electrons, thus enabling the electrons stored in GS to grow new small metal islands at different sites. Comparatively speaking, the Pt islands are more inclined to repel the electrons accumulation than Pd, thus making the Pd NPs grow larger and distribute more unevenly than Pt. Additionally, further increase of 200 μL Pd^{2+} and $PtCl_6^{2-}$ solution only led to aggregation of Pd and Pt NPs, while the increase in their particle sizes is almost negligible (Figure 2b and d). And the Pt NPs seem to form a kind of compact cluster. The above results conformed well with the mechanism in Scheme 1.

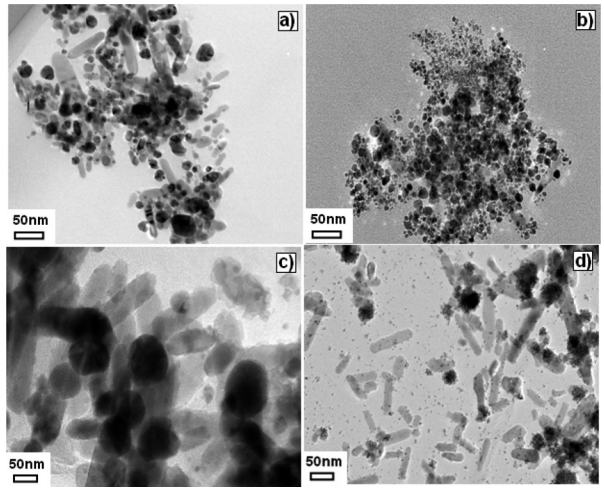

Figure 2. Typical TEM images of (a) GS/ZnO@Ag_{580}, (b) GS/ZnO@Pd_{580}, (c) GS/ZnO@Au_{580}, and (d) GS/ZnO@Pt_{580}.

Figure 3 presents X-ray diffraction (XRD) spectra of GS/ZnO@M_{380}, where the XRD patterns of ZnO nanorods and GS/ZnO/M_{380} are also shown for comparison. Apparently, almost all GS/ZnO@M_{380} samples exhibit the usual wurtzite structure, Just like original ZnO nanorods, with similar peak intensities and shapes, which shows 11 peaks at 31.7°, 34.4°, 36.2°, 47.5°, 56.6°, 62.9°, 66.4°, 68.0°, 69.1°, 72.6°, and 77.0°, indexed to (100), (002), (101), (102), (110), (103), (200),

dx.doi.org/10.1021/am401738k | ACS Appl. Mater. Interfaces 2013, 5, 6762−6768

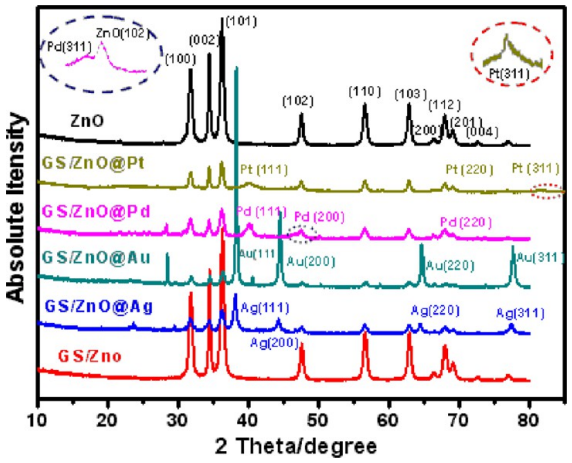

Figure 3. Typical XRD patterns of (a) ZnO, (b) GS/ZnO@Pt_{380}, (c) GS/ZnO@Pd_{380}, (d) GS/ZnO@Au_{380}, (e) GS/ZnO@Ag_{380}, and (f) GS/ZnO. (Inset graph is taken from the spots assigned on curves b and c.)

(112), (201), (004), and (202) planes of the ZnO crystal, respectively.[32,33] Furthermore, the observed peaks corresponding to the (111), (200), (220), and (311) facets of Ag, Pd, Au, and Pt were all assigned (JCPDS card), which demonstrated that Ag, Pd, Au, and Pt NPs are all composed of pure crystalline with the face-centered cubic (fcc) structure.[34−37] The intensity ratios of the (200) peak to the (111) peak obtained for the Ag (0.401), Pd (0.464), Au (0.346), and Pt indicate that Ag, Pd, Au, and Pt were preferentially dominated by (111) facets. The (200) peak for Pt cannot be assigned in this XRD pattern, which can be explained by considering that the (200) peak is overlapped with ZnO (102).

The chemical state of the metal in GS/ZnO@M_{380} has been examined by X-ray photoelectron spectroscopy (XPS). In Figure 4a, peaks located at 284.6, 285.4, and 288.7 eV are the deconvolution spectra from C 1s of GS/ZnO, corresponding to C−C, C−OH, and carboxylic groups O−C═O, respectively. The low intensity of the oxygen functional groups confirms the presence of reduction of GO into GS. The peak at binding energy of 1023 eV corresponds to the Zn ($2p_{3/2}$) and another one located at 1046 eV is attributed to the Zn ($2p_{1/2}$), which are identical to those of ZnO nanorods. For all the metal species, two peaks are observed, and no other peaks can be deconvoluted (Figure 4c−f). The data and the assignments of XPS spectra for the GS/ZnO@M_{380} composites definitely indicate that the photoelectric reduction has reduced the ionic metals into the metallic states.

Further characterization of GS/ZnO@M_{380} hybrid nanocomposites using electrochemical technique was also performed. The cyclic voltammograms of electron transfer indicator of $Fe(CN)_6^{3-/4-}$ were studied at four GS/ZnO@M_{380} modified electrodes. The comparison among them with respect to the peak-to-peak separations (ΔE_p) and the magnitude of peak current were also investigated together with GS/ZnO in Figure 5 (left). Compared with GS/ZnO, it can be clearly witnessed that GS/ZnO@M_{380} based electrodes all displayed higher magnitude of peak current and smaller ΔE_p value. Among the GS/ZnO@M_{380}, GS/ZnO@Pt_{380} (curve a) with the ΔE_p value of 169 mV shows the enhanced peak current compared with the other three with the ΔE_p values of 293 mV (Pd), 365 mV (Ag), and 460 mV (Au). The order of the peak currents is also coinciding with the ΔE_p sequence very

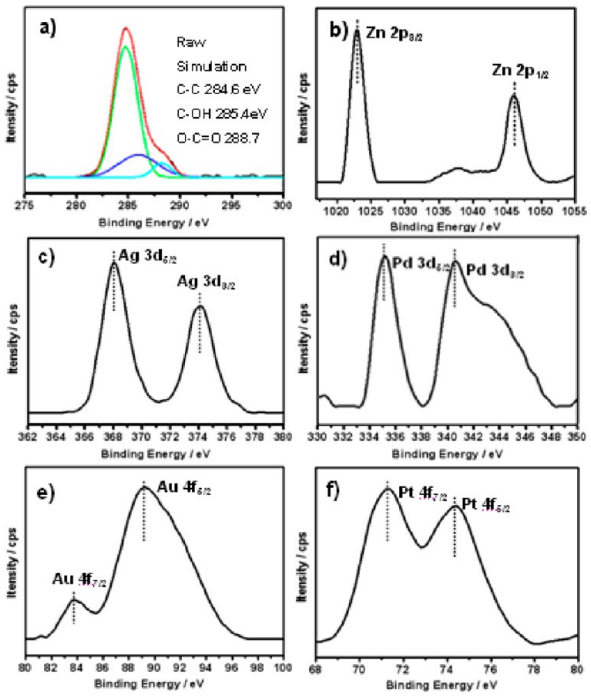

Figure 4. XPS spectra of (a) C1s and (b) Zn2p in GS/ZnO, and the photoelectric-reduced GS/ZnO@M composites: (c) GS/ZnO@Ag, (d) GS/ZnO@Pd, (e) GS/ZnO@Au, and (f) GS/ZnO@Pt.

well. Therefore, the above results reveal that electron transfer is more facilitated at GS/ZnO@Pt_{380} and GS/ZnO@Pd_{380} surfaces. Electrochemical impedance spectroscopy (EIS) further confirmed the above results. In Figure 5 (right), the charge-transfer resistance (R_{ct}) of the $Fe(CN)_6^{3-/4-}$ redox couple is near 3.4 kΩ at GS/ZnO substrate (curve e), and then it decreases to 2.78, 2.39, 1.75, and 1.46 kΩ at GS/ZnO@Au_{380}, GS/ZnO@Ag_{380}, GS/ZnO@Pd_{380}, and GS/ZnO@Pt_{380} substrate electrodes, respectively. The decreases in the charge-transfer resistance at GS/ZnO@M_{380} surfaces, particularly at GS/ZnO@Pt_{380} and GS/ZnO@Pd_{380} surfaces, intrinsically enhance the electron transfer, which is in good agreement with the results obtained in cyclic voltammetry.

Electrochemical Activity of GS/ZnO@M_{380} Nanocomposites. Most metal NPs electrocatalysts have been evaluated for both the methanol-oxidation and oxygen-reduction reactions.[38,39] In the light of the above fact that the diameters and distribution of the four respective resultant metal NPs on GS/ZnO exerted a significant difference, it is therefore of our interest to investigate what role these resultant GS/ZnO@M hybrid nanocomposites with different additive amounts of metal ions may play on the electrocatalytical behavior of some kind of substance. Here, we take H_2O_2 as the probe. Figure 6a presents the dependence of the current responses of GS/ZnO@M hybrid nanocomposites with different additive amounts of metal ions to 1.0 mM H_2O_2 on their specific peak potentials, which are recorded between −0.4 and +0.6 V by cyclic voltammetry at GS/ZnO@M_v based glassy carbon electrodes in 0.1 M PBS (pH 7.4). For GS/ZnO@Ag_v, GS/ZnO@Au_v, and GS/ZnO@Pt_v, the current value increases slightly with different additive amounts of metal ions, after which the growth speeds up and reaches the maximum at their specific amount. Taking GS/ZnO@Pt_v, for example, the current value increases slightly with adding the first 580 μL of H_2PtCl_6 in small increments, after which the growth speeds

dx.doi.org/10.1021/am401738k | ACS Appl. Mater. Interfaces 2013, 5, 6762−6768

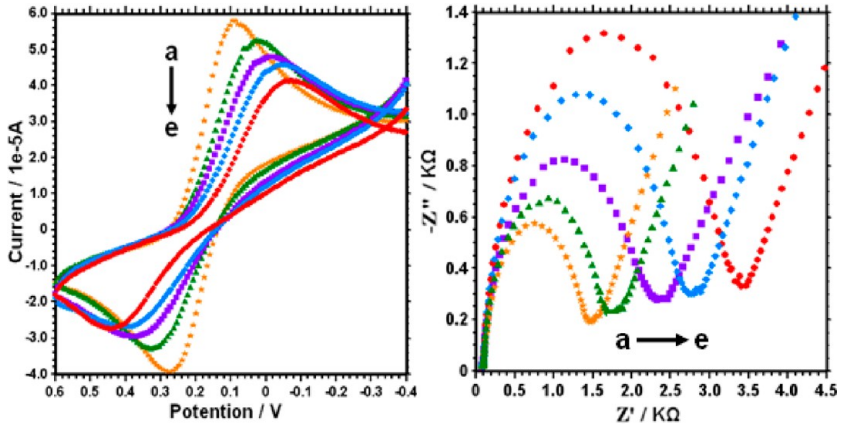

Figure 5. Cyclic voltammograms obtained at GS/ZnO and GS/ZnO@M_{380}-GC in 0.1 M KCl solution containing 1 mM $K_3Fe(CN)_6$ and Nyquist plots obtained at GS/ZnO and GS/ZnO@M_{380}-GC in 0.1 M KCl solution containing 1 mM $[Fe(CN)_6]^{3-/4-}$: (a) GS/ZnO@Pt380, (b) GS/ZnO@Pd380, (c) GS/ZnO@Ag380, (d) GS/ZnO@Au380, and (e) GS/ZnO.

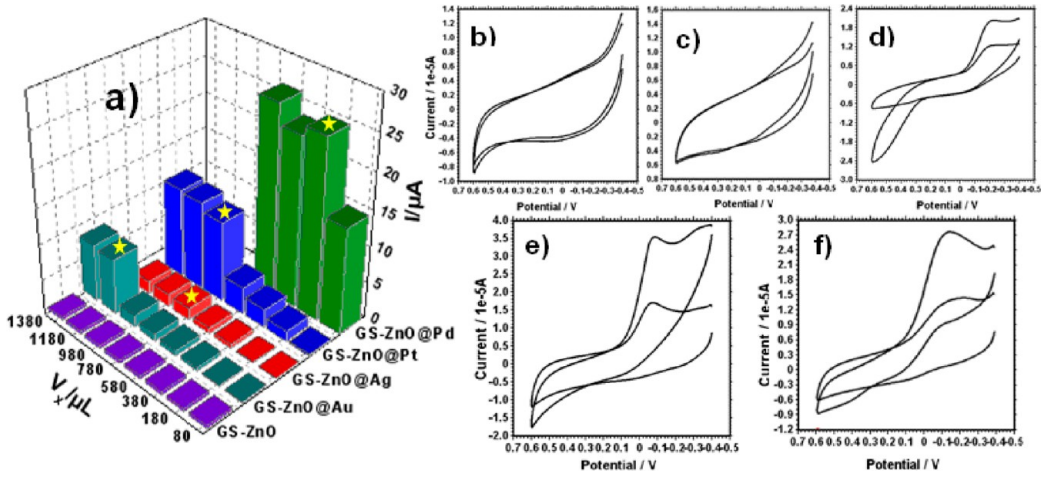

Figure 6. (a) Dependence of the responses of GS/ZnO@M_{380} hybrid nanocomposites modified electrodes to 1.0 mM H_2O_2 on their specific peak potentials with different additive amounts of metal ions: 80, 180, 380, 580, 780, 980, 1180, and 1380 μL. Comparison of cyclic voltammetry (CV) responses of the (b) GS/ZnO, (c) GS/ZnO@Ag_{780}, (d) GS/ZnO@Pd_{180}, (e) GS/ZnO@Au_{1180}, and (f) GS/ZnO@Pt_{780} modified electrodes in blank 0.1 M PBS (pH 7.4) (bottom line) and 1.0 mM H_2O_2 in PBS (above line).

up and reaches the maximum at GS/ZnO@Pt_{780}. As for the GS/ZnO@Pd_v nanocomposites, it is soon to come to saturation when adding only 180 μL of $PdCl_2$. The most active electrocatalytic behavior with the optimized amount of metal ions toward the reduction of H_2O_2 for GS/ZnO@M_v, as illustrated in Figure 6b–f, is GS/ZnO@Ag_{780}, GS/ZnO@Pd_{180}, GS/ZnO@Au_{1180}, and GS/ZnO@Pt_{980}, respectively. It can be explained by considering that, with the increasing the volume of the metal ion, the metal NPs' effective electroactive area of the electrode is increased and its electrochemical behavior is also improved. However, the further increase may lead to the aggregation of metal NPs, thus resulting in the counteractive effect on the electrocatalytic activity. In addition, we also found that, with the same addition volume of varied metal ions, GS/ZnO@Pd_{380} possessed the highest electrocatalytic activity toward H_2O_2 than GS/ZnO@Ag_{380}, GS/ZnO@Au_{380}, and GS/ZnO@Pt_{380}. It can be generally accepted that the four metals all have their intrinsic catalytic activity. And more importantly, the smaller size and more uniform distribution of the deposited Pd and Pt NPs based films provide higher electroactive surface area and thus substantially decreased the overpotential in the detection of H_2O_2, which caused the higher activities in the electrochemical performance of GS/ZnO@Pd and GS/ZnO@Pt observed here. Furthermore, the GS/ZnO@M may be an attractive robust and advanced hybrid electrode material with great promise for electrochemical sensors and biosensors design.

CONCLUSIONS

In this work, a series of metal NPs with different topography and diameter based on new functional graphene were successfully achieved via UV-assisted photocatalytic reduction through ZnO nanorods. Noble metal NPs embedded on GS/ZnO provided larger electroactive area, and electrochemical characteristics were improved. Therefore, taking H_2O_2 as the probe, we investigated the role that these resultant GS/ZnO@M hybrid nanocomposites with different additive amounts of metal ions may play on their electrocatalytical behavior. Furthermore, it should also be possible to control the particle size of metal NPs by controlling the proportion of of electron storage in graphene.

dx.doi.org/10.1021/am401738k | ACS Appl. Mater. Interfaces 2013, 5, 6762–6768

EXPERIMENTAL SECTION

Chemicals and Reagents. Graphite powder (GO, 99.5%, 325 mesh) was from Alfa Aesar. Silver nitrate ($AgNO_3$, 99.8%, 20 mg/mL), palladium dichloride ($PdCl_2$, 99.9%, 20 mg/mL), hydrogen tetrachloroaurate hydrate ($HAuCl_4 \cdot 3H_2O$, 99.9%, 20 mg/mL), hexachloroplatinic acid hexahydrate ($H_2PtCl_6 \cdot 6H_2O$, 99.9%, 1g/5 mL), and poly(*N*-vinyl-2-pyrrolidone) (PVP·K30, molecular weight = 30 000−40 000) were purchased from Shanghai Chemical Reagent Company (Shanghai, China). All other reagents and solvents were of analytical grade and used without further purification. Double-distilled water was used for preparation of all solutions and for washing.

Apparatus and Instruments. FT-IR spectra were obtained from Nicolet Nexus 670 spectrometer. UV−vis absorption spectra were recorded on CARY-50 Conc spectrometer. The morphologies of the as-prepared GS-ZnO as well as the corresponding GS-ZnO@M hybrid nanocomposites were studied on a scanning electron microscope (Hitachi Co. Ltd., Tokyo, Japan) and transmission electron microscope (JEOL 2010, operating at 200 KV). The XRD patterns were collected on a Bruker D8 ADVANCE instrument using Cu Kα radiation. The thermal decomposition temperatures (T_d) with a 5% weight loss were assessed by employing a TGA 851e/SF/1100 analyzer at a heating rate of 10 °C/min under flowing nitrogen atmosphere. Raman spectra were obtained on a J-Y T64000 Raman spectrometer with 514.5 nm wavelength incident laser light. X-ray photoelectron spectroscopy (XPS) experiments were carried out on a RBD upgraded PHI-5000C ESCA system (Perkin-Elmer) with Mg Kα radiation ($h\nu$ = 1253.6 eV) or Al Kα radiation ($h\nu$ = 1486.6 eV). Electrochemical experiments were performed on CHI 832B electrochemical workstation (CH Instrument) with a conventional three-electrode system composed of a platinum wire as counter electrode, a saturated calomel electrode (SCE) (Jiangsu Electroanalytical Instruments Factory, China) as reference electrode, and a bare or a modified glass carbon electrode as working electrode.

Preparation of GS/ZnO. ZnO nanorods were synthesized through a hydrothermal route. Typically, 4.45 mmol $Zn(CH_3COO)_2 \cdot 2H_2O$ was dissolved in 42 mL of methanol containing 250 μL of H_2O and heated to 70 °C. KOH (9.62 mmol) dissolved in 23 mL of methanol was added into the above solution over 10−15 min and then heated at 80 °C for 2 h. The resultant solution, which became white, was ultrasonically treated for 30 min in a water bath and then transferred into a Teflon-lined stainless autoclave and heated up to 180 °C for 72 h. The obtained white powder was ZnO nanorods. Graphite oxide was synthesized from graphite by a modified Hummers method.[16] the obtained GO was mixed with ethanol to yield a yellow-brown suspension and ultrasonicated until it became clear without particulate matter. A homogeneous GO dispersion (40 mg/mL) was used for further chemical reduction. In the typical process of preparing graphene/ZnO nanocomposite, 25 mL of GO suspension (40 mg/mL), 1 g of PVP, and 2 g of ZnO were first mixed together and stirred for 1.5 h, and then transferred into a Teflon-lined stainless autoclave and heated up to 180 °C for 3 h. After cooling to room temperature, the resulting ashen suspension was centrifuged and washed with ethanol several times and then dried under vacuum at 60 °C.

Preparation of GS-ZnO@M. Before self-assembly of M NPs on the surface of GS/ZnO with the assistance of UV-light, 25 mg of the GS/ZnO nanocomposite was first dispersed in 5 mL of ethanol and ultrasonicated to form a 5 mg/mL suspension. Then, a known amount of deaerated M^{n+} ($AgNO_3$, $PdCl_2$, $HAuCl_4$, and H_2PtCl_6) aqueous solution (20 mg/mL) was slowly added in small increments to the as-prepared deaerated GS-ZnO suspension under stirring. Finally, the resulting dispersion was exposed to UV-light for 30 min, during which M^{n+} was photoreduced to M^0.

Construction of GS-ZnO@M Modified Electrode. Glassy carbon electrode (2 cm × 1.5 cm) used in the electrochemical experiments was polished with alumina paste (0.05 μm) on a microcloth and subsequently ultrasonically cleaned thoroughly with acetone, NaOH (1:1), HNO_3 (1:1), and doubly distilled water and then dried at room temperature. Then, 2 μL of the above GS/ZnO@M suspension was dropped onto the cleaned bare electrode, being allowed to dry at ambient temperature. To get good redox peaks, the GS/ZnO@M_{380} suspension diluted three times was used to construct the electrode to perform the cyclic voltammetry of electron transfer indicators such as $Fe(CN)_6^{3-/4-}$.

ASSOCIATED CONTENT

Supporting Information

SEM and TEM images of the GS/ZnO, EDS of GS/ZnO confirming the presence of Zn in the composite film, representative Raman spectra, FTIR spectra, UV−vis spectra, TGA curves of GO and the obtained GS/ZnO. This material is available free of charge via the Internet at http://pubs.acs.org.

AUTHOR INFORMATION

Corresponding Author

*E-mail: gyshi@chem.ecnu.edu.cn.

Notes

The authors declare no competing financial interest.

ACKNOWLEDGMENTS

This work is supported by the National Natural Science Foundation of China (21175044, 21275055). This work is supported the Programs of the Science & Technology Commission of Shanghai Municipality (10JC1404000). We also greatly thank the Research Fund for the Doctoral Program of Higher Education (20100076110002)

ABBREVIATIONS

GS = graphene sheets
NPs = nanoparticles
IEP = high isoelectric point
PVP = polyvinyl pyrroliadone

REFERENCES

(1) Pang, M. L.; Hu, J. Y.; Zeng, H. C. *J. Am. Chem. Soc.* **2010**, 132.
(2) Liu, B.; Aydil, E. S. *J. Am. Chem. Soc.* **2009**, *131*, 3985−3990.
(3) Nie, L. H.; Yu, J. G.; Li, X. Y.; Cheng, B.; Liu, G.; Jaroniec, M. *Environ. Sci. Technol.* **2013**, *47* (6), 2777−2783.
(4) Shvalagin, V. V.; Stroyuk, A. L.; Kuchmii, S. Ya. *J. Nanopart. Res.* **2007**, *9*, 427−440.
(5) Tada1, H.; Mitsui1, T.; Kiyonaga1, T.; Akita, T.; Tanaka, K. *Nat. Mater.* **2006**, *5*, 782−786.
(6) Zhang, D. B.; Wang, S. J.; Cheng, K.; Dai, S. X.; Hu, B. B.; Han, X.; Shi, Q.; Du, Z. L. *ACS Appl. Mater. Interfaces* **2012**, *4*, 2969−2977.
(7) Shen, F. Y.; Que, W. X.; He, Y. C.; Yuan, Y.; Yin, X. T.; Wang, G. F. *ACS Appl. Mater. Interfaces* **2012**, *4*, 4087−4092.
(8) Park, H. Y.; Go, H. Y.; Kalme, S.; Mane, R. S.; Han, S. H.; Yoon, M. Y. *Anal. Chem.* **2009**, *81*, 4280.
(9) Yao, K. X.; Liu, X.; Zhao, L.; Zeng, H. C.; Han, Y. *Nanoscale* **2011**, *3*, 4195−4200.
(10) Claudia, P.; Andreas, K.; Horst, W. *Angew. Chem., Int. Ed.* **2004**, *43*, 4774−4777.
(11) Fan, X. F.; Zheng, W. T.; Kuo, J. L. *ACS Appl. Mater. Interfaces* **2012**, *4*, 2432−2438.
(12) Wu, X. M.; Hu, Y. J.; Jin, J.; Zhou, N. L.; Wu, P.; Zhang, H.; Cai, C. X. *Anal. Chem.* **2010**, *82*, 3589.
(13) Stankovich, S.; Dikin, D. A.; Dommett, G. H. B.; Kohlhaas, K. M.; Zimney, E. J.; Stach, E. A.; Piner, R. D.; Nguyen, S. T.; Ruoff, R. S. *Nature* **2006**, *442*, 282.
(14) Chen, J.; Bi, H.; Sun, S. R.; Tang, Y. F.; Zhao, W.; Lin, T. Q.; Wan, D. Y.; Huang, F. Q.; Zhou, X. D.; Xie, X. M.; Jiang, M. H. *ACS Appl. Mater. Interfaces* **2013**, *5*, 1408−1413.
(15) Xu, Y. X.; Bai, H.; Lu, G. W.; Li, C.; Shi, G. Q. *J. Am. Chem. Soc.* **2008**, *130*, 5856.
(16) Choi, B. G.; Park, H. S. *ChumSusChem* **2012**, *5*, 709−715.

(17) Guo, Y. J.; Guo, S. J.; Ren, J. T.; Zhai, Y. M.; Dong, S. J.; Wang, E. K. *ACS Nano* **2010**, *4*, 4001−4010.
(18) Bao, H. Q.; Pan, Y. Z.; Ping, Y.; Sahoo, N. G.; Wu, T. F.; Li, L.; Li, J.; Gan, L. H. *Small* **2011**, *7*, 1569−1578.
(19) Zhang, D.; Xie, F. X.; Lin, P.; Choy, W. H. *ACS Nano* **2013**, *7*, 1740−1747.
(20) Dimiev, A.; Kosynkin, D. V.; Slesarev, A.; Sun, Z.; Tour, J. M. *Science* **2011**, *331*, 1168−1172.
(21) Seger, G. B.; Kamat, P. V. *ACS Nano* **2008**, *2*, 1487−1491.
(22) Lightcap, I. V.; Kosel, T. H.; Kamat, P. V. *Nano Lett.* **2010**, *10*, 577−583.
(23) Liua, X. J.; Pana, L. K.; Zhao, Q. F.; Lva, T.; Zhua, G.; Chena, T. Q.; Lua, T.; Suna, Z.; Sunc, C. Q. *Chem. Eng. J.* **2012**, *183*, 238−243.
(24) Kamat, P. V. *J. Phys. Chem. Lett.* **2010**, *1*, 520−527.
(25) Mulvaney, P. *Langmuir* **1996**, *12*, 788−801.
(26) Ung, T.; Dunstan, D.; Giersig, M.; Mulvaney, P. *Langmuir* **1997**, *13*, 1773−1782.
(27) Wood, A.; Giersig, M.; Mulvaney, P. *J. Phys. Chem. B* **2001**, *105*, 8810−8815.
(28) Sanchez-Iglesias, A.; Carbo-Argibay, E.; Glaria, A.; Rodriguez-Gonzalez, B.; Perez-Juste, J.; Pastoriza-Santos, I.; Liz-Marzan, L. M. *Chem.—Eur. J.* **2010**, *16*, 5558−5563.
(29) Lu, Y.; Shi, C.; Hu, M. J.; Xu, Y. J.; Yu, L.; Wen, L. P.; Zhao, Y.; Xu, W. P.; Yu, S. H. *Adv. Funct. Mater.* **2010**, *20*, 3701.
(30) Zhang, Z. C.; Zhang, X.; Yu, Q. Y.; Liu, Z. C.; Xu, C. M.; Gao, J. S.; Zhuang, J.; Wang, X. *Chem.—Eur. J.* **2012**, *18*, 2639−2645.
(31) Guo, S. J.; Wen, D.; Zhai, Y. M.; Dong, S. J.; Wang, E. K. *ACS Nano* **2010**, *4*, 3959−3968.
(32) Walia, S.; Weber, R.; Balendhran, S.; Yao, D.; Abrahamson, J. T.; Zhuiykov, S.; Bhaskaran, M.; Sriram, S.; Strano, M. S.; Kalantar-zadeh, K. *Chem. Commun.* **2012**, *48*, 7462−7464.
(33) Garcia, M. A.; Merino, J. M.; Fernandez Pinel, E.; Quesada, A.; Venta, J. D. L.; Ruiz Gonzalez, M. L.; Castro, G. R.; Crespo, P.; Llopis, J.; Gonzalez-Calbet, J. M.; Hernando, A. *Nano Lett.* **2007**, *7*, 1489−1494.
(34) Zheng, Y. H.; Chen, C. Q.; Zhan, Y. Y.; Lin, X. Y.; Zheng, Q.; Wei, K. M.; Zhu, J. F. *J. Phys. Chem. C* **2008**, *112*, 10773−10777.
(35) Cheng, F. L.; Wang, H.; Sun, Z. H.; Ning, M. X.; Cai, Z. Q.; Zhang, M. *Electrchem. Commun.* **2008**, *10*, 798.
(36) Tian, Y.; Liu, H. Q.; Zhao, G. H.; Tatsuma, T. *J. Phys. Chem. B* **2006**, *110*, 23478−23481.
(37) Zhou, Y. G.; Chen, J. J.; Wang, F. B.; Sheng, Z. H.; Xia, X. H. *Chem. Commun.* **2010**, *46*, 5951−5953.
(38) Wang, L.; Nemoto, Y.; Yamauchi, Y. *J. Am. Chem. Soc.* **2011**, *133*, 9674−9677.
(39) Yu, Y. Y.; Sun, Q.; Liu, X. Q.; Wu, H. H.; Zhou, T. S.; Shi, G. Y. *Chem.—Eur. J.* **2011**, *17*, 11413−11323.